Catalytic and Structural Effects of Amino Acid Substitution at Histidine 30 in Human Manganese Superoxide Dismutase: Insertion of Valine Cγ into the Substrate Access Channel †

ARTICLE *in* BIOCHEMISTRY · APRIL 2003

Impact Factor: 3.02 · DOI: 10.1021/bi0266481 · Source: PubMed

8 AUTHORS, INCLUDING:

M. Elizabeth Stroupe
Florida State University
34 PUBLICATIONS **485** CITATIONS
SEE PROFILE

Diane E Cabelli
Brookhaven National Laboratory
99 PUBLICATIONS **3,130** CITATIONS
SEE PROFILE

Cecilia Ramilo
Somerset Community College
15 PUBLICATIONS **1,138** CITATIONS
SEE PROFILE

John Tainer
University of Texas MD Anderson Cancer Center
457 PUBLICATIONS **30,042** CITATIONS
SEE PROFILE

Articles

Catalytic and Structural Effects of Amino Acid Substitution at Histidine 30 in Human Manganese Superoxide Dismutase: Insertion of Valine Cγ into the Substrate Access Channel†

Amy S. Hearn,‡ M. Elizabeth Stroupe,§ Diane E. Cabelli,|| Cecilia A. Ramilo,‡ James P. Luba,‡ John A. Tainer,§ Harry S. Nick,‡ and David N. Silverman*,‡

Departments of Pharmacology and Neuroscience, University of Florida, Gainesville, Florida 32610-0267, Department of Molecular Biology, The Scripps Research Institute, 10550 North Torrey Pines Road, La Jolla, California 92037, and Chemistry Department, Brookhaven National Laboratory, Upton, New York 11973-5000

Received August 15, 2002; Revised Manuscript Received January 22, 2003

ABSTRACT: Catalysis of the disproportionation of superoxide by human manganese superoxide dismutase (MnSOD) is characterized by an initial burst of catalysis followed by a much slower region that is zero order in superoxide and due to a product inhibition by peroxide anion. We have prepared site-specific mutants with replacements at His30, the side chain of which lies along the substrate access channel and is about 5.8 Å from the metal. Using pulse radiolysis to generate superoxide, we have determined that k_{cat}/K_m was decreased and product inhibition increased for H30V MnSOD, both by 1−2 orders of magnitude, compared with wild type, H30N, and H30Q MnSOD. These effects are not attributed to the redox potentials, which are similar for all of these variants. An investigation of the crystal structure of H30V Mn(III)SOD compared with wild type, H30Q, and H30N Mn(III)SOD showed the positions of two γ carbons of Val30 in the active site; Cγ1 overlaps Cγ of His30 in wild type, and Cγ2 extends into the substrate access channel and occupies the approximate position of a water molecule in the wild type. The data suggest that Cγ2 of the Val side chain has significantly interrupted catalysis by this overlap into the access channel with possible overlap with the substrate−product binding site. This is supported by comparison of the crystal structure of H30V MnSOD with that of azide bound to Mn(III)SOD from *Thermus thermophilus* and by visible absorption spectra showing that azide binding to the metal in H30V Mn(III)SOD is abolished. Moreover, the presence of Val30 caused a 100-fold decrease in the rate constant for dissociation of the product-inhibited complex compared with wild type.

The superoxide dismutases catalyze the decay of superoxide through oxidation−reduction cycles of a metal ion. Manganese superoxide dismutase (MnSOD)[1] has an amino acid sequence and crystal structure very similar to FeSOD, but these have no homologies with CuZnSOD or NiSOD (*1*). Catalysis involves at least two stages, an oxidation stage and a reduction stage. The formation of the product hydrogen peroxide requires two protons which must ultimately come from solution at a rate at least as fast as the maximal catalytic turnover, which is near 40 ms^{-1} (*2*, *3*) (see Scheme 1). In this scheme Mn(III)SOD represents the manganese bound to the enzyme. The rates of various steps in this catalysis were measured using stopped-flow spectrophotometry by Bull et al. (*2*) for MnSOD from *Thermus thermophilus* and by Hsu et al. (*3*) for human MnSOD using pulse radiolysis. Both of these studies expanded on a previous investigation of catalysis by MnSOD from *Bacillus stearothermophilus* by McAdam et al. (*4*) that described an initial burst of catalysis followed rapidly, within milliseconds, by a region of decay which is zero order in superoxide, measured directly from the absorbance of $O_2^{\bullet -}$ at 250 nm. This was attributed to the reversible formation of an inactive form of the MnSOD most likely due to product inhibition, written as Mn−X−SOD in Scheme 1. Subsequently, Bull et al. (*2*) measured the visible absorption spectrum of MnSOD in the region of zero-order decay of superoxide and suggested that its

† This work was supported by grants from the American Lung Association (to A.S.H.) and the National Institutes of Health (GM54903 to D.N.S. and GM48495 to J.A.T.). The pulse radiolysis work was carried out at Brookhaven National Laboratory under Contract DE-AC02-98CH108816 with the U.S. Department of Energy and supported by its Division of Chemical Sciences, Office of Basic Energy Sciences.

* Address correspondence to this author at Box 100267 Health Center, University of Florida, Gainesville, FL 32610-0267. Phone: 352-392-3556. Fax: 352-392-9696. E-mail: silvermn@college.med.ufl.edu.

‡ University of Florida.

§ The Scripps Research Institute.

|| Brookhaven National Laboratory.

[1] Abbreviations: MnSOD, manganese superoxide dismutase; H30V MnSOD, the site-specific mutant of MnSOD in which His30 is replaced with Val; Mops, 3-(*N*-morpholino)propanesulfonic acid; Taps, *N*-[tris-(hydroxymethyl)methyl]-4-aminobutanesulfonic acid; Ches, 2-(*N*-cyclohexylamino)ethanesulfonic acid.

10.1021/bi0266481 CCC: $25.00
Published on Web 02/22/2003

Scheme 1

$$\text{Mn(III)SOD} + O_2\cdot^- \rightleftarrows [\text{Mn(III)SOD-}O_2\cdot^-] \rightarrow \text{Mn(II)SOD} + O_2$$

$$\text{Mn(II)SOD} + O_2\cdot^- + 2H^+ \rightleftarrows [\text{Mn(II)SOD-}O_2\cdot^-] + 2H^+ \rightarrow \text{Mn(III)SOD} + H_2O_2$$

$$\downarrow\uparrow$$

$$\text{Mn-X-SOD}$$

maximum at 420 nm was consistent with the formation of a side-on (bidentate) peroxo complex of the manganese. The product-inhibited nature of the complex was confirmed by Hearn et al. (*5*) by observing the same characteristic spectrum upon mixing human MnSOD with H_2O_2. Subsequent studies showed that the extent of product inhibition during catalysis was enhanced or diminished for various active site mutants of human MnSOD (*6*, *7*).

We report here significant changes in the extent of catalysis and of product inhibition of human MnSOD by site-specific mutagenesis at a single site, position 30. Residue 30 is histidine in the wild-type enzyme and is a highly conserved residue in all MnSODs and FeSODs. The side chain of His30 in human MnSOD is located about 5.8 Å from the manganese and participates in a hydrogen-bonded chain that extends from the manganese-bound solvent molecule to Tyr166 of the adjacent subunit and out to solution (*8*). In previous studies, Borders et al. (*9*) replaced His30 with Ala in *Saccharomyces cerevisiae* MnSOD and concluded that His30 does not play a crucial role in catalysis or stability. Ramilo et al. (*10*) replaced His30 of human MnSOD with several amino acids and observed catalysis and solved a crystal structure for H30N Mn(III)SOD. These substitutions were shown to interrupt the hydrogen bond network extending into the active site of wild-type MnSOD. Moreover, catalysis by H30N MnSOD was decreased 10-fold for k_{cat} and 6-fold for k_{cat}/K_m compared with wild type. Edwards et al. (*11*) measured catalysis by H30A MnSOD from *Escherichia coli* and found that it was reduced about 30−40% compared to wild type. They also obtained the crystal structure of this mutant at 2.2 Å resolution, which showed altered hydrogen bonding and significant conformational changes in backbone atoms.

We show here that the replacement of His30 with Val in human MnSOD resulted in a mutant with much decreased catalytic activity and was very susceptible to product inhibition compared with wild-type, H30N, and H30Q MnSOD. The values of the midpoint potential were not substantially altered in any of these variants. Rather, an investigation of the crystal structure of H30V compared with wild-type, H30Q, and H30N MnSOD suggests that a Cγ of the side chain of Val30 has significantly interrupted catalysis by steric overlap with the substrate−product binding site or the substrate access channel. This is supported by comparison of the crystal structures of human H30V MnSOD and the azide-inhibited complex of *T. thermophilus* MnSOD and studies showing that azide binding to H30V MnSOD is abolished.

METHODS

PCR-Based Site-Directed Mutagenesis. Human MnSOD cDNA [cDNA sequence reported by Beck et al. (*12*)] was amplified using a pair of oligonucleotide primers, GCATATGAA GCACAGCCTCC and GGAGATCTCAGCATAACGATC. The plasmid pHMNSOD4 (ATCC no. 59947) which contains human MnSOD was subcloned into the TA cloning vector PCRII (Invitrogen Corp.). A series of primers were designed to create the mutants H30X in human MnSOD (X = N, Q, V). A pair of oligonucleotides, primer 1 (5′ CCTAGTAATCATTTCATGAAGCACAGCCTCCCCG 3′) and primer 2 (5′ CTGCAGAATACAGTAAGCTGC 3′) were used to recreate the entire MnSOD coding region. For each mutant, two oligonucleotides designated as primer 3 (5′ CAGCTGCACCATTCGAAGGTCCACGCGGCCTA 3′) and primer 4 (5′ TAGGCCGCGTGGACCTTCGAATGGTGCAGCTG 3′) were made, whose sequences are complementary to each other and contain the mutation of interest at position 30 (underlined for H30V). Two separate PCR reactions were used to amplify the 5′ half (primers 1 and 4) and 3′ half (primers 3 and 2) of the MnSOD cDNA coding sequence. The PCR products from these reactions were purified by initially running gel electrophoresis, followed by the removal of contaminants on the excised band using the Qiagen gel purification kit (Qiagen Corp.). To create the whole coding region, another round of PCR was carried out using the purified PCR products as template with primers 1 and 2. The PCR products which now contained the mutation at position 30 of the cDNA coding region were purified as described above and then cut with the restriction enzymes *Bsp*HI and *Pst*I. Restriction sites *Bsp*HI and *Pst*I were incorporated into primers 1 and 2, respectively. Cloning was accomplished by ligating the cohesive ends of the vector and the PCR-derived mutant cDNA MnSOD gene. The N-terminal portion of the protein which contained the *Bsp*HI site was ligated to the compatible *Nco*I end in PTrc 99A (Pharmacia Corp.), recreating an ATG codon, and the C-terminal end of the cDNA was annealed to the *Pst*I site of the vector. Small-scale expression of the mutant protein was done on the selected clones to verify protein expression by the clone, and correct incorporation of the desired altered base was verified by DNA sequencing of both the top and bottom strands of the purified plasmid. The constructs expressed human MnSOD as mature proteins in the mutant $SodA^-/SodB^-$ *E. coli* (strain QC774) and tagged with an extra methionine at the amino terminus. Culture conditions included 0.1−1.0 mM $MnCl_2$. Yields of human MnSOD mutant protein were on average 50−200 mg of protein/12 L of bacterial culture.

Purification. Mutants of human MnSOD were purified from *E. coli* using heat treatment and ion-exchange chromatography [DE52 (anion exchanger) and CM52 (cation exchanger), Whatman Corp.)] according to the procedures of Beck et al. (*13*) with some modifications. The modification included the use of another cation exchanger, SP-Sepharose

(Pharmacia Corp.), whenever necessary. Heat treatment was also reduced to 30 min and 55 °C for the less stable mutants. The purity of the protein was checked at various stages of purification using SDS−PAGE. The purified protein showed a unique intense band. Each mutant was dialyzed extensively with EDTA and passed through a desalting column (PD 10, Pharmacia Corp.) before analysis for manganese content using inductively coupled plasma (ICP) or atomic absorption spectrophotometry. The concentration of the active enzyme was taken as the manganese concentration [ϵ_{480} for Mn(III)SOD is 600 ± 20 M^{-1} cm^{-1}; *17*]. The fraction of active sites occupied by manganese varied from 0.68 for H30N to 0.76 for wild type. Protein concentrations were determined by the Lowry method.

Pulse Radiolysis. The pulse radiolysis experiments were carried out using the 2 MeV van de Graaff accelerator at the Brookhaven National Laboratory. The amount of superoxide generated during pulse radiolysis was established using the KSCN dosimeter, assuming that $(SCN)_2^-$ has a G value of 6.13 and molar absorptivity of 7950 $M^{-1}cm^{-1}$ at 472 nm. All UV/vis spectra were recorded on a Cary 210 spectrophotometer at a constant temperature of 25 °C. The path length was either 2.0 or 6.1 cm. Solutions contained enzyme, 30 mM sodium formate (as a hydroxyl radical scavenger) (*14*), 50 mM EDTA, and a 2 mM quantity of one of the following buffers: Mops (pH 7.2), Taps (pH 8.2), and Ches (pH 9.2). Superoxide radicals were generated in situ by introducing nanosecond pulses to aqueous, air-saturated solutions containing sodium formate according to the mechanisms described by Schwarz (*14*). Under these conditions, the formation of $O_2{\cdot}^-/HO_2$ radicals is more than 95% complete by the first microsecond after the pulse. The decay of superoxide was monitored spectrophotometrically at 260 nm (ϵ_{260} = 1800 M^{-1} cm^{-1}; *15*).

Scanning Stopped-Flow Spectrophotometry. The catalysis by MnSOD and the mutant enzymes H30Q, H30N, and H30V was observed by scanning stopped-flow spectrophotometry (Applied Photophysics Ltd., SX.18MV) in a sequential mixing experiment in which KO_2 in a solution of dimethyl sulfoxide and 18-crown-6 ether (*16*) was diluted (1:10) in two sequential rapid mixings. The final solution contained 0.25 mM enzyme, 1 mM $O_2{\cdot}^-$, 1.0 mM EDTA, and 100 mM Ches buffer at pH 9 and 8.3% (by volume) dimethyl sulfoxide. The change in absorbance of the enzyme with time from 350 to 700 nm was monitored spectrophotometrically.

Azide Binding to MnSOD. The binding of azide to MnSOD and mutants was investigated using scanning stopped-flow spectrophotometry (Applied Photophysics Ltd., SX.10MV) in a single mixing experiment. The final solutions contained 0.25 mM enzyme, 20 mM KH_2PO_4 at pH 7.8, and 50 μM EDTA. Azide concentration was varied up to 125 mM. The visible absorbance of the enzyme was observed between 350 and 700 nm.

Reduction of MnSOD by H_2O_2 and Dithionite. The reduction of MnSOD and mutants by H_2O_2 and dithionite was measured using scanning stopped-flow spectrophotometry (Applied Photophysics Ltd., SX.10MV) in a single mixing experiment. For hydrogen peroxide reduction, the final solution contained 0.25 mM enzyme, 25 mM H_2O_2, 20 mM KH_2PO_4 at pH 7.8, and 50 μM EDTA. Reductions with dithionite contained 0.25 mM enzyme, 2.5 mM dithionite, 20 mM KH_2PO_4 at pH 7.8, and 50 μM EDTA. The reductions were followed spectrophotometrically between 350 and 700 nm.

Table 1: Diffraction Data and Refinement Statistics for Wild-Type, H30V, and H30Q Human MnSODs

	WT	H30V	H30Q
resolution (Å)	20−1.8 (1.88−1.85)[a]	20−1.82 (1.89−1.82)	17−2.3 (2.34−2.3)
R_{free} (%)	28.8	24.0	27.8
% test reflections	10	10	9
R_{cryst} (%)	25.4	22.4	23.4
unique reflections	39262	41609	19640
redundancy	4.5	7.3	2.06
I/σ	13.4 (3.3)[a]	36.0 (5.6)	7.4 (2.6)
R_{merge} (%)	7.8 (46)[a]	7.9 (28)	7.5 (33)
% completeness	98 (99)[a]	99.4 (99.1)	93 (91)
no. of atoms (non-H)	3146	3140	3142
no. of solvent molecules	325	337	195

[a] Highest resolution bin.

Redox Potential Measurements. Measurements of the midpoint potential E_m of human H30V MnSOD were performed by single point experiments; enzyme and mediator were allowed to equilibrate from opposite redox states as described in Lévêque et al. (*17*) at pH 8.0. Solutions of enzyme were exchanged into 20 mM Taps and 100 mM KCl through three cycles of concentration and dilution using Centricon-10 filters. Once buffer exchange was completed, the solution was diluted to 3 mL, resulting in 0.3−0.4 mM H30V MnSOD. The solution was sealed in an anaerobic cell with a combination electrode and made anaerobic through several cycles of vacuum and N_2 gas. MnSOD was partially reduced by 0.3 mM H_2O_2 and 0.27 mM $K_3Fe(CN)_6$. The absorbance spectra and redox potential of the system were measured every hour for up to 24 h. Absorbance at 421 nm (ferricyanide) and 485 nm [H30V Mn(III)SOD] was plotted against redox potential, and the midpoint potential E_m was determined through least-squares fits (Enzfitter, Biosoft) of the Nernst equation. The midpoint potential of H30V MnSOD was also measured using 0.4 mM pentacyanoaminoferrate as the mediator. Similar procedures were used to determine E_m for H30Q MnSOD. Midpoint potentials are reported versus the normal hydrogen electrode.

Crystallography of H30V, H30Q, and Wild-Type MnSOD. Crystals grew from 2−3 M ammonium sulfate at pH 7−8, buffered by 100 mM imidazole/malate. Data were collected on crystals flash frozen in the liquid nitrogen stream after they were washed in mother liquor containing 20% ethylene glycol. The wild-type and H30V data sets were collected on beamline 9-1 at the Stanford Synchrotron Radiation Laboratory using a Mar345 detector. The data for H30Q MnSOD were collected at the Protein Structure Facility at the University of California, San Diego, from a Cu Kα rotating anode X-ray source, using a Mar345 detector to record the images. Data were processed and reduced using Denzo/Scalepack (*18*). The structures were solved by rigid-body refinement against the Y34F structure (*19*), and the structures were refined using CNS (*20*). Diffraction data and refinement statistics are presented in Table 1. R_{free} reflections were randomly flagged for 10% of the data across all resolution shells. The structure was manually fit against ($2F_o - F_c$)

Table 2: Values of the Steady-State Kinetic Constants, the Zero-Order Rate Constant k_0/[E] for the Product-Inhibited Phase, and the Midpoint Potential E_m for Wild-Type Human MnSOD and Three Mutants at Position 30

enzyme	k_{cat} (ms^{-1})	k_{cat}/K_m ($\mu M^{-1}\ s^{-1}$)	k_0/[E] (s^{-1})	E_m (mV)
wild type	40[a]	800[a]	500	393 ± 29[d]
H30N	4.3[b]	130[b]	2000	365 ± 28[d]
H30Q	1.4[b]	52[b]	660	380 ± 30[e]
H30V	−[c]	3	2	457, 475[e] 440[f]

[a] From Hsu et al. (*3*). [b] From Ramilo et al. (*10*). [c] This enzyme was extensively inhibited, and we have not measured this rate constant accurately. [d] From Lévêque et al. (*17*). [e] Measurements using ferricyanide as mediator. [f] One measurement using pentacyanoaminoferrate as mediator.

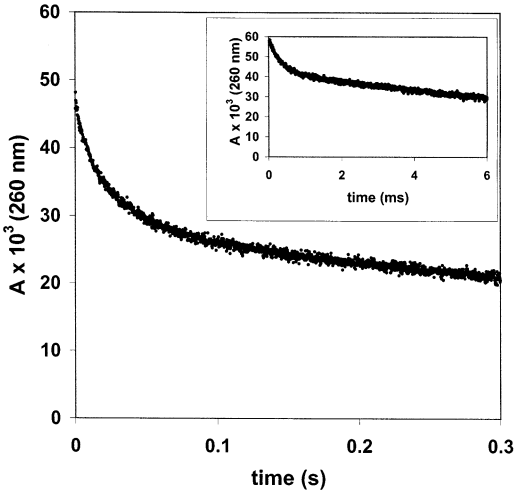

FIGURE 1: Decrease in absorbance of superoxide at 260 nm (path length 2 cm) during catalysis by 5.0 μM H30V MnSOD. The initial concentration of $O_2\cdot^-$ was 13 μM generated by pulse radiolysis. Solutions at 25 °C also contained 30 mM formate, 50 μM EDTA, and 2 mM Taps at pH 9.2 and were equilibrated with air. Inset: Catalysis by 1.0 μM human wild-type MnSOD with the initial concentration of $O_2\cdot^-$ at 16 μM. Other conditions are as described above.

and ($F_o - F_c$) maps calculated in CNS and displayed using the XtalView suite (*21*). Coordinates were deposited in the Protein Data Bank with the following accession codes: 1NON for H30V MnSOD; 1LUV for wild-type MnSOD at 1.85 Å; and 1LUW for H30Q MnSOD.

RESULTS

Catalysis. The decay of superoxide catalyzed by wild-type MnSOD has been well characterized as an initial burst of catalyzed dismutation followed by a region of decay that is zero order in superoxide and attributed to product inhibition (*2*, *3*). The zero-order rate constant for this region of the decay, k_0/[E], was determined to be 500 s^{-1} for human wild-type MnSOD (Table 2; *7*). Using pulse radiolysis to generate superoxide, we measured the decrease in absorbance of superoxide at 260 nm catalyzed by H30V MnSOD. Figure 1 demonstrates the initial burst followed by the inhibited region during catalysis by H30V MnSOD; it can be compared to the much less inhibited wild type in which the catalytic burst was observed for about 1 ms after introduction of superoxide and before the inhibited region (inset to Figure 1; see also ref 3). Like inhibition of wild-type MnSOD (*2*, *3*), the inhibited region for H30V MnSOD can be described as a zero-order process (Figure 1) with a zero-order rate constant k_0/[E] = 2 s^{-1}. In Table 2 this value of k_0/[E] is compared with that observed during catalysis by wild type and two other site-specific mutants at position 30: H30N and H30Q MnSOD. The extent of product inhibition for H30Q MnSOD was similar to that of wild-type MnSOD (*3*) and weakest for H30N MnSOD (Table 2).

Since introduction of superoxide by pulse radiolysis does not involve a mixing time, the initial velocity of superoxide decay before inhibition was accessible and used to estimate steady-state constants. These values for the position 30 mutants are compared with the more efficient wild type in Table 2. The ratio k_{cat}/K_m for H30V MnSOD was more than 2 orders of magnitude smaller than wild type. The extent of product inhibition of H30V MnSOD was so great that we could not accurately measure catalysis at the high superoxide concentrations required to determine k_{cat}.

Product inhibition was also studied by scanning stopped-flow spectrophotometry. The absorbance profiles from 350 to 750 nm of H30V and H30Q MnSOD were obtained under identical conditions using 0.25 mM enzyme and 1 mM $O_2\cdot^-$. Figure 2 shows such profiles at 6.4 ms after mixing [these can be compared with the spectrum of wild-type MnSOD presented in the inset of Figure 2; see also Hearn et al. (*5*)]. The peak at 420 nm, which is characteristic of the product-inhibited complex, is very distinct in H30V MnSOD in contrast to the much smaller peak for the less inhibited H30Q MnSOD. For H30V MnSOD, the 420 nm peak did not decay completely even after several seconds, while for H30Q the 420 nm peak had completely decayed by 50 ms.

We then used pulse radiolysis to follow the rate of appearance and disappearance of the 420 nm peak and were able to estimate rate constants in a simplified mechanism. The McAdam scheme (eqs 1−4) is a simple pathway that

$$\text{Mn(III)SOD} + O_2\cdot^- \xrightarrow{k_1} \text{Mn(II)SOD} + O_2 \quad (1)$$

$$\text{Mn(II)SOD} + O_2\cdot^- \xrightarrow{k_2\,(+2H^+)} \text{Mn(III)SOD} + H_2O_2 \quad (2)$$

$$\text{Mn(II)SOD} + O_2\cdot^- \xrightarrow{k_3} \text{Mn}-\text{X}-\text{SOD} \quad (3)$$

$$\text{Mn}-\text{X}-\text{SOD} \xrightarrow{k_4\,(+2H^+)} \text{Mn(III)SOD} + H_2O_2 \quad (4)$$

has been used to explain catalysis and product inhibition by MnSOD (*4*); it makes few assumptions concerning the identity of species and role of proton transfer. In eqs 1−2, individual steps in the catalytic cycle are considered irreversible, justified in part by the favorable equilibrium constants associated with these reactions. Equations 3 and 4 represent the formation and dissociation of the product-inhibited complex. The advantage of eqs 1−4 for this work is that they simplify the catalytic cycle of eqs 1 and 2 while emphasizing the formation and dissociation of the inhibited complex Mn−X−SOD in eqs 3 and 4. This mechanism has been applied to human wild-type MnSOD and adequately describes catalysis and product inhibition (*22*).

We have used pulse radiolysis to introduce $O_2\cdot^-$ into solution containing H30V Mn(II)SOD (reduced by H_2O_2) and have observed the increase in absorbance at 420 nm

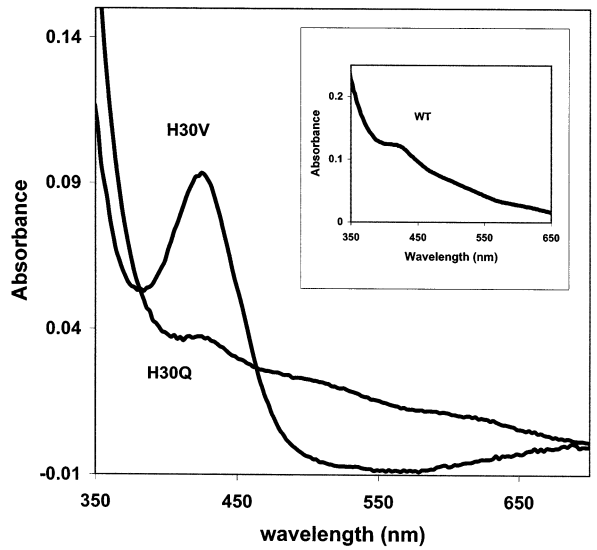

FIGURE 2: Absorbance spectrum of H30V MnSOD and H30Q MnSOD measured by scanning stopped-flow spectrophotometry 6.4 ms after mixing at an initial concentration of 1.0 mM superoxide. Solutions at 20 °C contained 0.25 mM enzyme, 0.1 mM EDTA, and 200 mM Ches at pH 9.0. Spectra have been corrected for background absorbance by subtraction of absorbance at 730 nm. Inset: Absorbance spectrum of wild-type MnSOD measured under identical conditions.

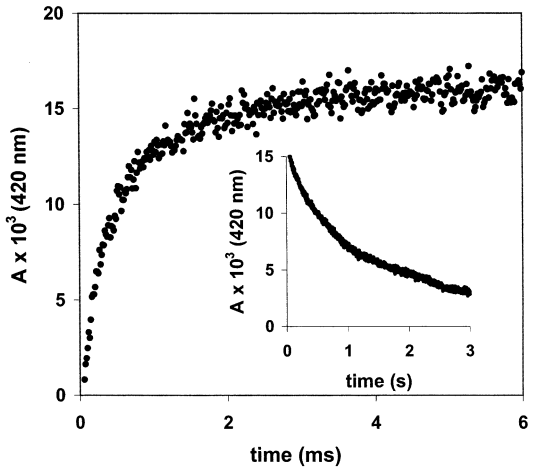

FIGURE 3: Increase of absorbance at 420 nm during the catalysis of superoxide decay caused by the emergence of the inhibited complex of 20 μM H30V MnSOD. The initial concentration of $O_2\cdot^-$ was 4.8 μM, generated by pulse radiolysis. Solutions at 25 °C also contained 30 mM formate, 50 μM EDTA, and 2 mM Taps at pH 8.2 and were equilibrated with air. H30V MnSOD was reduced by introduction of H_2O_2 before the experiment. Inset: Decrease in absorbance at 420 nm under the same conditions but over a much longer time that measures the decay of the inhibited complex of H30V.

indicating the emergence of the inhibited state. The formation and decay of the 420 nm absorption allowed us to obtain the rate constants k_3 and k_4 of eqs 3 and 4. Figure 3 shows the increase in absorbance at 420 nm for the inhibited complex of H30V MnSOD measured over a short time scale after introduction of superoxide by pulse radiolysis. The inset to Figure 3 shows the decrease in this absorbance as the inhibited complex decays over a much longer time scale. The rate constants resulting from these and similar measurements on H30N, H30Q, and wild-type MnSOD are presented in Table 3. Here, comparison with the other variants shows

Table 3: Values of the Rate Constants of Eqs 1−4 for Catalysis by MnSOD and Mutants Obtained by Direct Observation of the Absorbance of the Free Oxidized Enzyme at 480 nm and the Inhibited Enzyme at 420 nm[a]

enzyme	k_1 (μM^{-1} s^{-1})	k_2 (μM^{-1} s^{-1})	k_3 (μM^{-1} s^{-1})	k_4 (s^{-1})
wild type	1500	1100[b]	1100[b]	120
H30N	210	400[b]	680[b]	480
H30Q	570	790[b]	790[b]	200
H30V	~5[c]	~30[c]	160	0.7

[a] Solutions contained 5 μM mutant enzymes or 1 μM wild-type enzyme equilibrated in air and also contained 30 mM formate, 50 mM EDTA, and 2 mM Mops buffer at pH 7.8 or 2 mM Taps buffer at pH 8.2. All data are at 25 °C. [b] Values of k_2 and k_3 are very close and were difficult to differentiate. [c] H30V was strongly product-inhibited, and fitting of progress curves for catalysis showed that the simplified mechanism of eqs 1−4 was inadequate to describe the kinetics. Hence, these values must be considered very approximate.

that, in forming the inhibited complex, k_3 for H30V MnSOD (eq 3) is smaller by at most 4-fold compared with the other mutants of Table 3; however, in the dissociation of the inhibited complex k_4 for H30V (eq 4) is smaller by at least 2 orders of magnitude.

The rate constants k_1 and k_2 were more difficult to estimate for H30V MnSOD in large part because they are much smaller than k_3 (Table 3). Fitting the data for emergence and decay of absorptions at 420 nm and at 480 nm [the maximum in the visible absorption of wild-type Mn(III)SOD] was ambiguous and may signify the presence of enzyme species not represented in eqs 1−4. Further work is in progress on this topic.

Human wild-type Mn(III)SOD upon reduction with H_2O_2 passes transiently through a complex with a maximum absorbance at 420 nm decaying to Mn(II)SOD, which has no appreciable absorbance over the visible range (Figure 4; *5*). H30V MnSOD was reduced by H_2O_2 without evidence of an absorption at 420 nm (Figure 4). Under these same conditions, wild-type Mn(III)SOD was reduced by 2.5 mM dithionite with a half-time of 0.3 s; H30V Mn(III)SOD was not reduced under these conditions.

Azide inhibition. Hearn et al. (*5*) and Whittaker and Whittaker (*23*) noted that the visible absorption spectrum of the azide−MnSOD complex has a maximum near 420 nm; the data for the azide complex with wild-type human MnSOD is shown in Figure 5. This feature is also observed in the spectrum of the product-inhibited complex of H30V MnSOD (Figure 2); however, the visible spectrum of this product-inhibited complex lacks an absorbance shoulder near 500 nm that is observed in the azide adduct of *E. coli* MnSOD (*23*) and is represented as a broad absorbance in the azide adduct of human MnSOD (Figure 5). We estimate an apparent binding constant of azide of 2.2 ± 0.2 mM under the conditions of Figure 5 from the intensity of the absorbance at 420 nm upon equilibration of azide with human wild-type Mn(III)SOD. The binding constants for azide to H30N and H30Q MnSOD were 2.6 ± 0.6 mM and 1.8 ± 0.5 mM, respectively. In a range of azide concentrations up to 125 mM under the same conditions, there was no change in the absorbance spectrum of H30V MnSOD, which is very similar to that of wild type (Figure 5). We conclude that azide does not bind to the metal of H30V MnSOD in the range of azide concentrations used.

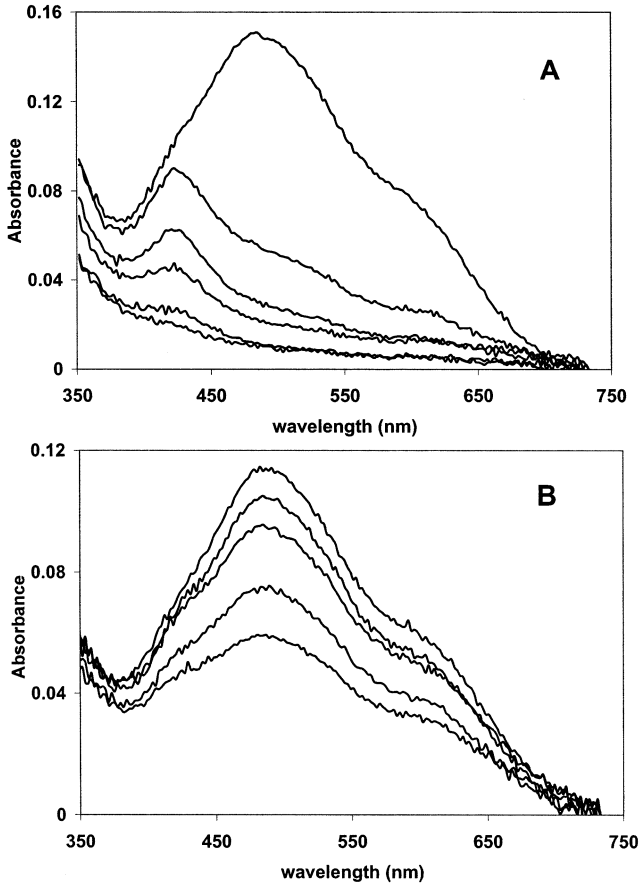

FIGURE 4: (A) Reduction by hydrogen peroxide of wild-type MnSOD measured by stopped-flow spectrophotometry. The upper curve shows the enzyme in the absence of H_2O_2; the remaining spectra from the top are at 11 ms, 100 ms, 500 ms, 2 s, and 10 s after introduction of 25 mM H_2O_2. Concentrations after mixing were 0.25 mM enzyme, 25 mM H_2O_2, and 20 mM phosphate buffer at pH 7.8 and 25 °C. (B) Reduction by hydrogen peroxide of H30V MnSOD. The upper curve shows the enzyme in the absence of H_2O_2; the remaining spectra from the top are at 100 ms, 2 s, 5 s, and 10 s after introduction of 25 mM H_2O_2. Other conditions are as above.

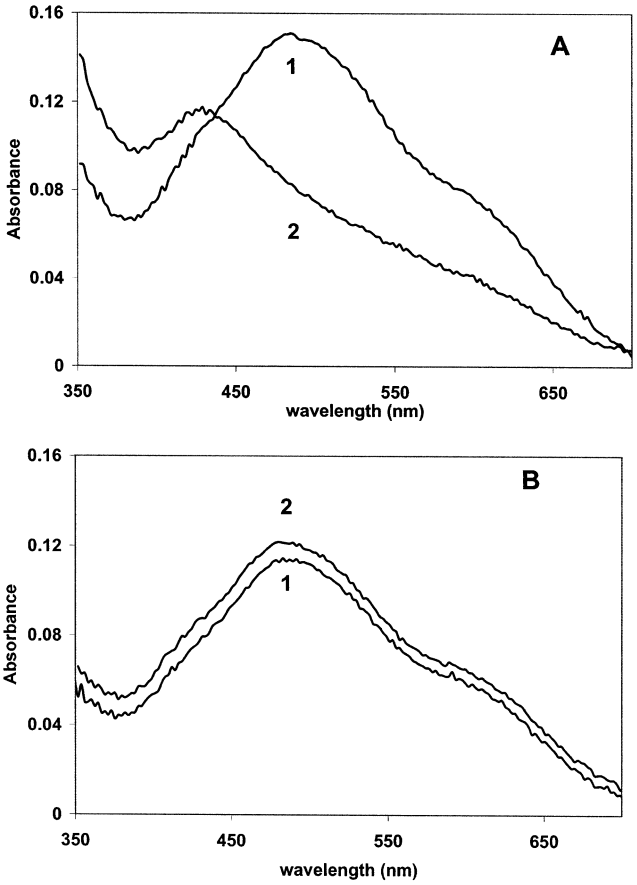

FIGURE 5: (A) Visible absorption spectra of wild-type MnSOD in the absence (curve 1) and presence (curve 2) of 125 mM azide. In each measurement enzyme was present at 0.25 mM in 20 mM phosphate buffer at pH 7.8 and 25 °C. (B) Visible absorption spectra of H30V MnSOD in the absence (curve 1) and presence (curve 2) of 125 mM azide. Other conditions are as above.

Redox Potential. The use of ferricyanide and pentacyanoaminoferrate as mediators in the measurement of the redox potential of human MnSOD has been described by Lévêque et al. (*17*). These mediators were applied to human H30V and H30Q MnSOD in single point experiments in which mediator and enzyme were allowed to equilibrate from opposite redox states. The two mediators (ferricyanide and pentacyanoaminoferrate) were used in separate experiments to calculate the intrinsic redox potentials of H30V and H30Q MnSOD. Redox equilibration between fully oxidized mediator and partially reduced enzyme (reduced with hydrogen peroxide) was slow, with a half-time near 6 h. We observed the change in absorption due to the reoxidation of enzyme at 485 nm and the corresponding reduction of ferricyanide at 421 nm. The ambient potential and the ratio of concentrations of oxidized to reduced forms of enzyme were substituted into the Nernst equation to obtain the midpoint potentials (E_m) of human H30V and H30Q MnSOD. Results in Table 2 show that the midpoint potential E_m for H30V is higher by about 70 mV for H30V compared with wild type. This indicates a slight difference in values of E_m between these variants of MnSOD, although the experimental uncertainty is high. The redox potentials of H30N and H30Q are much closer to the value of the wild type (Table 2).

Crystal Structure. Crystals in the space group $P6_122$ had unit cell dimensions of 79 Å × 79 Å × 240 Å for all three variants. The crystal structures of H30V Mn(III)SOD (Figure 6), H30Q Mn(III)SOD (data not shown), and H30N Mn(III)SOD (*10*) establish that the mutations at position 30 cause no significant changes on the overall structure of the enzyme. The root-mean-square difference for Cα atoms between wild type and H30Q was 0.42 Å and between wild type and H30V was 0.32 Å. Gln143, Tyr34, and Tyr166 are in the same conformation in both of the mutants H30V and H30Q as they are in the wild-type structure. These residues, together with ordered water molecules, form the hydrogen-bonded network that extends away from the aqueous ligand of the manganese to solvent, and they are believed to be catalytically important (*6*, *10*, *19*).

When superimposed, the human wild-type Mn(III)SOD and the H30V mutant show a nearly identical first shell of ligands around the active site manganese, including the Mn-bound solvent molecule (Wat1 of Figure 6). Also similarly superimposed are the side chains of two residues of the hydrogen bond network, Gln143 and Tyr34, as well as the torsional angle χ_1 representing the Cα−Cβ bond for residue 30. The major difference between the structures is that Val30 has a branched β carbon. One of these methyl groups, Cγ1 (Figure 6), overlaps the Cγ of His30 in the wild type [and

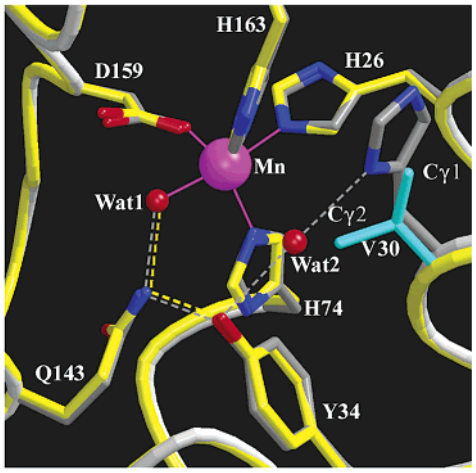

FIGURE 6: Least-squares superposition of the crystal structures of human wild-type (gray) and H30V Mn(III)SOD (yellow with Val30 colored blue). The ligands of the metal are His26, His74, His163, and Asp159. A water (Wat2) molecule hydrogen-bonded to His30 and Tyr34 was not observed in the mutant structure.

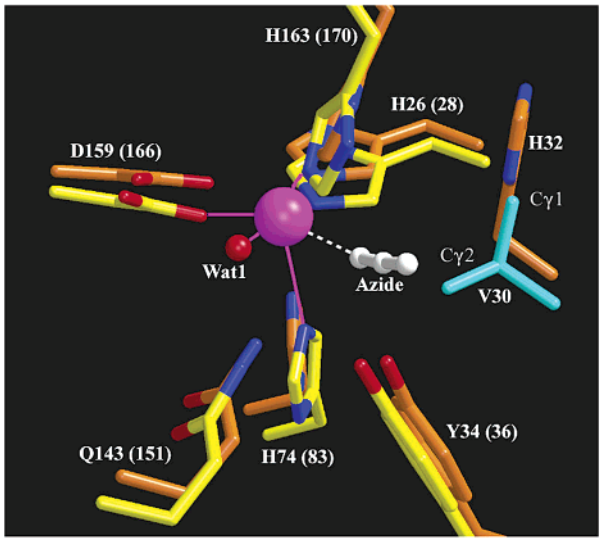

FIGURE 7: Least-squares superposition of the crystal structures of the complex of azide with Mn(III)SOD from *T. thermophilus* (orange with azide in white) [from the structure of Lah et al. (*25*)] and human H30V Mn(III)SOD (yellow with Val30 colored blue). The residue numbers in parentheses are for Mn(III)SOD from *T. thermophilus*; His32 of *T. thermophilus* is labeled without parentheses.

overlaps the Cγ of Gln30 in the crystal structure of H30Q Mn(III)SOD; data not shown]. The second methyl group of Val30, Cγ2, extends into the active site channel in the direction of Tyr34 (Figure 6). The 1.8 Å electron density map of Val30 shows a single rotamer for this side chain; other rotamers are hindered by potential interactions between side-chain methyl groups and the backbone carbonyl of one of the ligands of the metal, His26. As a result, the channel leading to the active site is more narrow in the H30V mutant than in the wild type. The distance from this Cγ2 of Val30 to the manganese is 4.4 Å; the distance from the hydroxyl oxygen of Tyr34 is 4.1 Å. In the wild-type Mn(III)SOD, the closest distance between the side chains of Tyr34 (hydroxyl oxygen) and the imidazole ring of His30 is 4.9 Å, representing a larger channel for possible approach of substrates and release of products.

There is a water molecule hydrogen-bonded to the side chains of both His30 and Tyr34 in wild-type Mn(III)SOD (Wat2 of Figure 6) that maintains the network of hydrogen-bonded residues that is believed to facilitate proton transfer in catalysis (*1*, *10*). Both H30Q and H30V lack this water molecule in their crystal structures; H30N has a water molecule between the side chains of Asn30 and Tyr34, but there is no hydrogen bond between Asn30 and this water (*10*). Hence evidence is consistent with the interruption of the hydrogen-bonded network in these mutations at residue 30; this may reduce the efficiency of proton transfer and account for the smaller values of k_{cat} for mutants at position 30 (Table 2). In wild-type MnSOD the side chain of His30 is also hydrogen-bonded to the side chain of Tyr166, which emanates from the adjacent subunit. This hydrogen bond is not possible for H30V; for H30N it is also lacking due to the altered orientation and shorter length of the Asn30 side chain. This arrangement is somewhat complicated in the crystal structure of H30Q MnSOD. There are two conformations of the Gln30 side chain, one in each subunit. In one, the hydrogen bond to Tyr166 is formed and in the other the hydrogen bond occurs to Tyr166 but through an intervening hydrogen-bonded water molecule. Thus in each of the mutants H30V, H30Q, and H30N there is altered hydrogen bonding to Tyr166. Since Tyr166 emanates from an adjacent subunit, these changes in hydrogen bonding to Tyr166 represent alterations at the interface between subunits. The influence of this feature on catalysis is not fully explored; however, in the mutant Y166F the value of k_{cat} is smaller by 10-fold than that of wild type (*10*).

DISCUSSION

The replacement of His30 in wild-type MnSOD with Val has caused a significant decrease in catalysis and increase in product inhibition, quite different than seen with the more conservative replacements by Asn and Gln. These changes upon amino acid substitution cannot be attributed to the rather small change in the redox potential of H30V MnSOD. However, our data provide several significant features to understand the very small catalytic activity of H30V MnSOD compared with wild type, H30N, and H30Q. The crystal structure of H30V MnSOD shows that a side-chain methyl group of Val30 (Cγ2) points into the active site cavity toward Tyr34 but causes no shift in the position of the side chain of Tyr34 (Figure 6); it is located about 4.4 Å away from the manganese.

To help to understand the implications on catalysis of Val30, we compare the structure of human H30V Mn(III)SOD with that of the azide-bound Mn(III)SOD from *T. thermophilus* (*25*) (Figure 7), azide being a substrate analogue. In *T. thermophilus* MnSOD, the azide binds to the metal through an end-on ligation expanding the coordination geometry about the manganese. The terminal nitrogen forms a hydrogen bond with the hydroxyl of Tyr34 and is 3.3 Å from the Nδ1 of His30 (numbering as in human MnSOD). Superimposing the azide-bound *T. thermophilus* MnSOD and human H30V MnSOD shows that the central nitrogen of the azide would interact unfavorably with Cγ2 of Val30; the distance between Cγ2 of Val30 and N2 of the azide is 2.1 Å and the van der Waals radius of a methyl group is near 2.0 Å. The azide-bound complex of *T. thermophilus* MnSOD shows that binding of azide requires

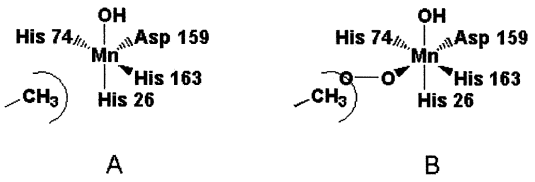

FIGURE 8: (A) Model showing the approximate trigonal-bipyramidal coordination about the manganese in H30V MnSOD. The Cγ2 methyl of Val30 is represented. (B) Model for an octahedral coordination of substrate bound to H30V MnSOD based on the distorted octahedral geometry about the manganese in *E. coli* MnSOD at 100 K (*26*). The model shows a steric hindrance of the Cγ2 methyl group of Val30 at the substrate binding site.

slight movement of residues in the active site cavity including Tyr34. Given the lack of constraints on Tyr34 in the H30V structure, including loss of a hydrogen bond with residue 30, it is likely that Tyr34 could make space for azide binding. Val30, on the other hand, is likely constrained by the backbone carbonyl of His26 and would come into unfavorable contact between Cγ2 and this carbonyl oxygen if it were to rotate about χ_1 to make space for azide.

Azide binds in a different mode in *E. coli* FeSOD (*25*), forming an end-on ligation to the metal and expanding its coordination geometry. Here azide appears to interact with the side chain of His74 and is located about 3.4 Å distant from the carbonyl oxygen of His26. Although the active site of human MnSOD is more similar to the *T. thermophilus* MnSOD, if azide were to bind to human MnSOD in a manner similar to that of the iron-containing enzyme, the middle nitrogen of the azide would still come into unfavorable contact with the Cγ2 of Val30, at an interatomic distance near 2 Å. These observations provide an explanation for the lack of binding of azide to human H30V MnSOD.

The Val30 Cγ2 of H30V Mn(III)SOD appears to lie directly on the substrate entry channel and may hinder the approach to and release of product in both the reduction (eq 1) and oxidation (eq 2) cycles of catalysis. Since azide is a substrate analogue, these data suggest an explanation for the very weak catalysis of superoxide dismutation by H30V MnSOD; specifically, the Cγ methyl group may block the substrate access channel and/or sterically overlap the substrate binding site, as it does for azide binding. This in significant part may account for the low value of k_{cat}/K_m for H30V compared with the other variants of Table 2; in these other mutants the single Cγ at residue 30 does not protrude into the substrate channel but superimposes with Cγ1 of wild type.

These observations are consistent with the lack of binding of the substrate analogue azide to human H30V MnSOD under conditions in which azide readily binds at the metal of the wild-type enzyme and support the suggestion that the mutation H30V may have decreased accessibility to the active site. A related possibility is that the Cγ2 methyl of Val30 could increase the barrier to the transition state through unfavorable steric overlap with the developing product peroxide. This is depicted in Figure 8B, showing a nearly octahedral complex caused by the addition of superoxide and its possible overlap with Cγ2 of Val30. The distorted octahedral complex is based on the structure of *E. coli* Mn(III)SOD at 100 K determined by Borgstahl et al. (*26*) in which the two solvent molecules are inner-shell ligands of the metal; in Figure 8B we assume substrate has displaced one of the solvent molecules. The five-coordinate, trigonal-bipyramidal structure in the absence of substrate found near room temperature is shown in Figure 8A (*8*). The observations that reduction of H30V MnSOD with H_2O_2 proceeds without an apparent absorption at 420 nm (Figure 4) and that H30V MnSOD is resistant to reduction by dithionite may be related to poor accessibility in the active site channel or steric overlap of the side chain of Val30 and binding sites at the metal.

Another possibility for the very low rate of catalysis by H30V MnSOD may be that a reduced efficiency of protonation of product at the active site is caused by the protrusion of the side-chain methyl group of Val30 into the access channel. One observation in support of this suggestion is that the rate constant k_3 describing the reaction of Mn(II)SOD to form the inhibited complex (eq 3) is still quite fast, near 160 μM^{-1} s^{-1}, for H30V MnSOD (Table 3). This is much more rapid than k_{cat}/K_m for H30V MnSOD near 3 μM^{-1} s^{-1} (Table 2). These data suggest that the formation of the inhibited complex is not as greatly affected by overlap with the Cγ2 of Val30 in H30V as is the catalytic cycle itself. The rapid formation of the inhibited complex of H30V, represented by k_3, would occur if the inhibited complex were, for example, a side-on complex of the peroxo dianion with the metal, the formation of which does not involve protonation. A less likely possibility is that the access channel for formation of the inhibited complex is different from the access channel of substrate in the catalytic pathway and is less hindered by Val30.

Upon replacement of His30 with Val, the rate constant for dissociation of the inhibited complex k_4 is lower in H30V MnSOD by a factor of over 100 compared with wild type, H30Q, and H30N (Table 3). Hearn et al. (*22*) established that k_4 is proton transfer dependent with a solvent hydrogen isotope effect near 2 in wild type and mutants at several positions including human H30N MnSOD. The crystal structure of wild-type MnSOD established the presence of a hydrogen bond network involving a number of side chains and solvent molecules (*8*): Mn−solvent−Gln143−Tyr34−solvent−His30−Tyr166, in which Tyr166 originates in the adjacent subunit of the dimer. The mutants H30V, H30N, and H30Q all interrupt this hydrogen bond network. Hence, this interruption by itself cannot account for the much decreased value of k_4 for H30V compared with H30Q and H30N MnSOD. However, the Cγ methyl group of Val30 may provide very strong inhibition by more thoroughly interrupting proton transfer and thus blocking a pathway for release of the inhibited complex.

ACKNOWLEDGMENT

We are grateful to David Duda for assistance in the preparation of Figures 6 and 7. We thank Ke Ren for excellent technical assistance. We acknowledge a referee's suggestion that the low value for the rate constant for dissociation of peroxide in H30V MnSOD may be due to the interruption by Val30 of proton transfer to the coordinated peroxo species. Portions of this research were carried out at the Stanford Synchrotron Radiation Laboratory, a national user facility operated by Stanford University on behalf of the U.S. Department of Energy, Office of Basic Energy Sciences. The SSRL Structural Molecular Biology Program

is supported by the Department of Energy, Office of Biological and Environmental Research, and by the National Institutes of Health, National Center for Research Resources, Biomedical Technology Program, and the National Institute of General Medical Sciences.

REFERENCES

1. Miller, A. F., and Sorkin, D. L. (1997) *Comments Mol. Cell. Biophys. 9*, 1−48.
2. Bull, C., Niederhoffer, E. C., Yoshida, T., and Fee, J. A. (1991) *J. Am. Chem. Soc. 113*, 4069−4076.
3. Hsu, J. L., Hsieh, Y., Tu, C. K., O'Connor, D., Nick, H. S., and Silverman, D. N. (1996) *J. Biol. Chem. 271*, 17687−17691.
4. McAdam, M. E., Fox, R. A., Lavelle, F., and Fielden, E. M. (1977) *Biochem. J. 165*, 71−79.
5. Hearn, A. S., Tu, C. K., Nick, H. S., and Silverman, D. N. (1999) *J. Biol. Chem. 274*, 24457−24460.
6. Hsieh, Y., Guan, Y., Tu, C. K., Bratt, P. J., Angerhofer, A., Lepock, J. R., Hickey, M. J., Tainer, J. A., Nick, H. S., and Silverman, D. N. (1998) *Biochemistry 37*, 4731−4739.
7. Cabelli, D. E., Guan, Y., Lévêque, V., Hearn, A. S., Tainer, J. A., Nick, H. S., and Silverman, D. N. (1999) *Biochemistry 38*, 11686−11692.
8. Borgstahl, G. E. O., Parge, H. E., Hickey, M. J., Beyer, W. F., Hallewell, R. A., and Tainer, J. A. (1992) *Cell 71*, 107−118.
9. Borders, C. L., Bjerrum, M. J., Schirmer, M. A., and Oliver, S. G. (1998) *Biochemistry 37*, 11323−11331.
10. Ramilo, C. A., Lévêque, V., Guan, Y., Lepock, J. R., Tainer, J. A., Nick, H. S., and Silverman, D. N. (1999) *J. Biol. Chem. 274*, 27711−27716.
11. Edwards, R. A., Whittaker, M. M., Whittaker, J. W., Baker, E. N., and Jameson, G. B. (2001) *Biochemistry 40*, 4622−4632.
12. Beck, Y., Oren, R., Amit, B., Levanon, A., Gorecki, M., and Hartman, J. R. (1987) *Nucleic Acids Res. 15*, 9076.
13. Beck, Y., Bartfeld, D., Yavin, Z., Levanon, A., Gorecki, M., and Hartman, J. R. (1988) *Bio/Technology 6*, 930−935.
14. Schwarz, H. A. (1981) *J. Chem. Educ. 58*, 101−105.
15. Rabani, J., and Nielson, S. O. (1969) *J. Phys. Chem. 73*, 3736−3744.
16. Valentine, J. S., and Curtis, A. B. (1975) *J. Am. Chem. Soc. 97*, 224−226.
17. Lévêque, V. J.-P., Vance, C. K., Nick, H. S., and Silverman, D. N. (2001) *Biochemistry 40*, 10586−10591.
18. Otwinowski, Z., and Minor, W. (1997) *Methods Enzymol. 276*, 307−326.
19. Guan, Y., Hickey, M. J., Borgstahl, G. E. O., Hallewell, R. A., Lepock, J. A., O'Connor, D., Hsieh, Y., Nick, H. S., Silverman, D. N., and Tainer, J. A. (1998) *Biochemistry 37*, 4722−4730.
20. Brunger, A. T., Adams, P. D., Clore, G. M., Delano, W. L., Gros, P., Grosse-Kunstleve, R. W., Jiang, J. S., Kuszewski, J., Nilges, N., Pannu, N. S., Read, R. J., Rice, L. M., Simonson, T., and Warren, G. L. (1998) *Acta Crystallogr. D54*, 905−921.
21. McRee, D. E. (1992) *J. Mol. Graphics 10*, 44−47.
22. Hearn, A. S., Stroupe, M. E., Cabelli, D. E., Lepock, J. R., Tainer, J. A., Nick, H. S., and Silverman, D. N. (2001) *Biochemistry 40*, 12051−12058.
23. Whittaker, M. M., and Whittaker, J. W. (1996) *Biochemistry 35*, 6762−6770.
24. Esnouf, R. M. (1997) *J. Mol. Graphics 15*, 132−134.
25. Lah, M. S., Dixon, M. M., Pattridge, K. A., Stallings, W. C., Fee, J. A., and Ludwig, M. L. (1995) *Biochemistry 34*, 1646−1660.
26. Borgstahl, G. E. O., Pokross, M., Chehab, R., Sekher, A., and Snell, E. H. (2000) *J. Mol. Biol. 296*, 951−959.

BI0266481